Supporting Information for

Co_3O_4 nanoparticle water-oxidation catalysts made by pulsed-laser ablation in liquids

James D. Blakemore, Harry B. Gray, Jay R. Winkler, and Astrid M. Müller

Beckman Institute, and Division of Chemistry and Chemical Engineering, California Institute of Technology, M/C 139-74, Pasadena, California 91125; correspondence should be addressed to astridm@caltech.edu.

1. General Experimental Conditions and Apparatus

Materials and Methods

Pulsed laser ablation in liquids synthesis and liquid suspension absorption measurements were carried out in the Beckman Institute Laser Resource Center (California Institute of Technology). X-ray photoelectron spectroscopy and solid-state absorption measurements were performed at the Molecular Materials Research Center (Beckman Institute at California Institute of Technology). Transmission electron micrographs were collected at the Beckman Resource Center for Transmission Electron Microscopy and the Kavli Nanoscience Institute (California Institute of Technology).

All chemicals were used as received. Deionized water was obtained from a Barnstead Diamond Nanopure system and had a resistivity of ≥16 MΩ cm.

Synthesis

Nanomaterials were synthesized using the method of pulsed laser ablation in liquids. For each sample 0.5 g of Co powder (Aldrich, <150 μm) and 10 mL deionized water were stirred using a magnetic stirrer in a 30 mL glass beaker at room temperature in ambient air. A 355 nm, 8 ns pulse laser beam, provided by the third harmonic of a 10 Hz Q-switched Nd:YAG laser (Spectra-Physics Quanta-Ray PRO-Series), was focused with a 100 mm focal length plano-convex quartz lens 0.5 mm below the surface of the liquid. Each sample was irradiated for 60 minutes. Laser pulse energies were varied from 30 to 210 mJ/pulse. For synthesis of nanoparticles without N_2 present during the ablation, the water-Co-powder mixture was purged with Ar for 45 minutes, and the beaker was placed under an Ar blanket during laser irradiation. Beakers were thoroughly cleaned with *aqua regia* before use. After synthesis nanoparticle suspensions were separated from Co metal using a strong magnet. Synthesis under Ar purge in de-aerated water yields Co_3O_4 nanoparticles that are virtually identical with those synthesized in ambient air, ruling out nitrogen incorporation as giving rise to the yellow color. Syntheses with various irradiation times (30, 60, 90, and 120 minutes) yielded virtually identical Co_3O_4 nanoparticles, ruling out changes to the suspended Co_3O_4 nanoparticles by reabsorption of laser light.

Electrodeposited cobalt oxide catalyst was prepared according to the procedure published by Kanan and Nocera.[1] In detail, we passed 450 μC current with an applied voltage of 1.105 V vs. NHE through an aqueous solution of 0.5 mM $Co(NO_3)_2 \cdot 6H_2O$ (Aldrich) and 0.1 M pH 7.0 sodium phosphate buffer (made from monobasic and dibasic sodium phosphate, EM Science and Mallinckrodt, respectively) to electrodeposit cobalt oxide catalyst on a freshly cleaved highly-ordered pyrolytic graphite (HOPG) electrode; an Ag/AgCl/3.0 M NaCl reference electrode (Bioanalytical Systems, Inc.; measured to be +0.212 V vs NHE, reference electrode calibration is described below) and a Ni gauze (Alfa) counter electrode were used. Before catalytic activity testing the electrodeposited films were thoroughly washed with deionized water.

Characterization

UV-visible absorption measurements of nanoparticle suspensions were carried out using a Hewlett Packard spectrophotometer in 1 mm pathlength quartz cuvettes, while those of solid nanoparticle films drop-cast on glass and dried on air were performed in transmission mode using a Cary 5000 UV-Vis spectrophotometer equipped with an integrating sphere using a $BaSO_4$ white reference.

X-ray photoelectron spectra (XPS) were taken using a Surface Science Instruments M-probe surface spectrometer. Monochromatic Al Kα radiation (1486.6 eV) was used to excite electrons from the samples, which had been drop-cast on clean Cu or Ti foil and dried on air at room temperature. The sample chamber was maintained at $<5\times10^{-9}$ Torr. Survey scans from 0 to 1000 eV were carried out to identify the elements present in the nanoparticles. Binding energies were referenced to the C 1s peak arising from adventitious carbon, taken to have a binding energy of 285 eV. High-resolution spectra were collected for the Co 2p region.

Transmission electron microscopy (TEM) and electron diffraction measurements were performed using an FEI Tecnai F-30 or FEI Tecnai T-12. Samples were drop-cast on 200 mesh Cu grids coated with Formvar carbon (Ted Pella), which had been plasma-ionized immediately before sample preparation to improve wetting. Residual water was removed from the grids with filter paper after 45 seconds. The average diameter of the nanoparticles was determined using the ImageJ software.[2]

Cobalt content in the aqueous nanoparticle suspensions was analyzed using an HP-4500 Series inductively coupled plasma mass spectrometry (ICP-MS) instrument, which was calibrated using a concentration standard. Samples were diluted by a factor of 100 with 2% nitric acid before injection into the instrument. The measured values were used to determine catalyst mass loadings on electrodes, since a known volume was used to prepare each electrode.

Raman spectra were measured at room temperature using a Renishaw M1000 micro-Raman spectrometer with 514.5 nm laser excitation and a 50× magnification objective. A 10-mm slit was used, resulting in 4 cm^{-1} resolution. The measured Raman shifts were calibrated against a Si standard.

Cyclic voltammetry measurements were carried out at room temperature using a Gamry Reference 600 potentiostat/galvanostat. Current density *versus* potential data were collected using a standard single-compartment three-electrode electrochemical cell, with a Ni gauze (Alfa) counter electrode. An HOPG (GraphiteStore, surface area: 0.09 cm^2) working electrode was used to evaluate catalytic activity. The electrode consisted of an HOPG cube with 3 mm edge length, to whose back a silver-coated copper wire was firmly attached with silver paint. For mechanical stability the wire was run inside a glass tube, whose end and the sides of the HOPG block were sealed with an epoxy adhesive (Loctite Hysol 9460). An Hg/HgO reference electrode (CH Instruments) was used in aqueous 1.0 M pH 14.0 potassium hydroxide electrolyte. The current density *versus* potential data were not corrected for any uncompensated resistance losses. All potentials reported here are relative to the normal hydrogen electrode (NHE). All scans were taken at 100 mV/s. Before use working electrodes were cleaned by sonication for 10 minutes in concentrated hydrochloric acid, washing with deionized water, and their surfaces were polished using 200 and 600 grit sandpaper, after which the graphite was cleaved with adhesive tape to obtain a fresh HOPG surface for each catalyst tested.

The potential of the 1 M KOH Hg/HgO reference electrode was measured at room temperature to be $E = 0.934$ V vs. the reversible hydrogen electrode (RHE), thus corresponding to 0.107 V vs. NHE. The measurement was carried out in a single-compartment three-electrode electrochemical cell, with a Ni gauze counter electrode. For the RHE, a glassy carbon electrode with crystalline Pt nanoparticles attached to it was used instead of Pt wire because the increased Pt surface area facilitates hydrogen equilibration. The Pt nanoparticles were prepared similar to a procedure published by Feliu and co-workers,[3] with the exception that 5 equivalents ascorbic acid were used to reduce Pt ions instead of hydrogen gas.[4] Research-grade hydrogen was bubbled through the vigorously stirred aqueous 1.0 M pH 14.0 potassium hydroxide electrolyte for 10 minutes to reach hydrogen saturation at 1 atm H_2, which was monitored by recording the open-circuit potential *versus* time. Cyclic voltammetry of the hydrogen evolution reaction on Pt with a scan rate of 10 mV/s was employed to obtain the potential of the 1 M KOH Hg/HgO reference electrode vs. RHE.

Rotating ring-disk electrode electrochemistry (RRDE) measurements were carried out in a 100 mL three-neck round-bottom flask with a Princeton Applied Research Parstat 4000 and VersaStat 3 configured to operate as a bipotentiostat and a Pine MSR variable speed rotator used at 1,500 rpm. The electrolyte was aqueous 1.0 M pH 14.0 potassium hydroxide (Mallinckrodt); an Hg/HgO reference electrode (CH Instruments) and a Ni gauze (Alfa) counter electrode were used. The disk electrode was made of HOPG with stabilizing epoxy around its side (surface area: 0.07 cm^2), and the ring electrode consisted of platinum. The disk and ring electrodes were used in a Pine ChangeDisk assembly; in our configuration, the oxygen-detection collection efficiency is 12.8%. For RRDE experiments, the disk electrode potential was swept from 0.107 V to 0.767 V vs. NHE, while the ring electrode potential was held at -0.193 V vs. NHE. Before use the HOPG disk working electrode was cleaned as described above. For preparation of the Tafel plots the same conditions were used; the dwell time at each applied potential point was 5 minutes.

Long-term stability measurements were performed using a standard single-compartment three-electrode electrochemical cell, with an HOPG working electrode, a Ni gauze (Alfa) counter electrode, and an Hg/HgO reference electrode (CH Instruments), while the electrolyte was 1.0 M pH 14.0 aqueous potassium hydroxide. A Princeton Applied Research Parstat 4000 potentiostat was used for chronoamperometry experiments. A voltage of 0.857 V vs. NHE was applied for over 6 hours and the current was recorded. Rapid stirring was afforded by using the same RRDE instrument with a Pine MSR variable speed rotator used at 1,500 rpm as described above, with the exception that the Pt ring was not connected.

Faradaic yield of oxygen evolution was measured using a custom-built glass cell equipped with a photoluminescence-quench oxygen sensor (Neofox, Ocean Optics) and a Princeton Applied Research Parstat 4000 potentiostat. The O_2 concentration in the headspace (69 mL) of this glass cell, filled with 55 mL of 1.0 M pH 14.0 aqueous potassium hydroxide, was measured using an O_2-sensitive fluorescent patch (HIOXY, Ocean Optics). This patch was glued to the sealed end of a glass tube, inside which the instrument's optical fiber was placed. This glass tube assembly was placed in the headspace of the glass cell. A two-point calibration was used for the oxygen sensor, one point being 0% O_2 after 10 minutes argon-purge and the other being 20.9% O_2 in ambient air. An Hg/HgO reference electrode (CH Instruments), a Ni wire counter electrode (connected to the main chamber of the glass cell via a side arm) and an HOPG working electrode (either blank or with 360 ng Co_3O_4 nanoparticles synthesized at 90 mJ/pulse drop cast onto it) were used. All electrodes and the sensor patch glass tube were sealed against oxygen leakage into the cell with O-rings and internal glass threads (Ace Glass-Threds). The main working chamber was water-jacketed and kept at a constant temperature of (24.5±0.5)°C using a circulation chiller (mgw Lauda-Brinkmann RM 3) with a thermostat (mgw Lauda T-2) to ensure a stable response from the O_2 sensor.

Data analysis and graphing was performed with Igor Pro 6.22 (Wavemetrics).

2. Materials Characterization

The absorption spectrum of Co_3O_4 nanoparticles in aqueous suspension synthesized at 90 mJ/pulse is shown in Figure S1. It exhibits a broad band centered at 392 nm on a scattering background. In the inset are photos of commercially available bulk Co_3O_4 powder (black) and Co_3O_4 nanoparticles in aqueous suspension and as a thin film on plastic (yellow).

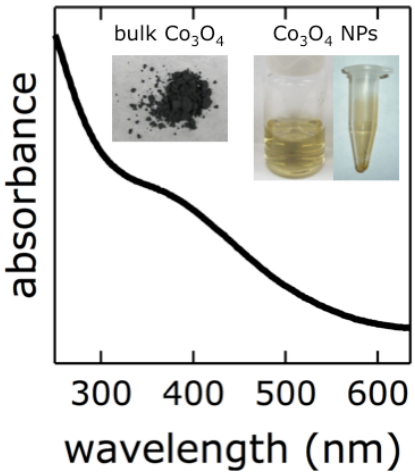

Figure S1: Absorption spectrum of Co_3O_4 nanoparticles in aqueous suspension synthesized using PLAL at 90 mJ/pulse. Inset: Photos of bulk Co_3O_4 powder from Aldrich (black) and Co_3O_4 nanoparticles (NPs) in aqueous suspension and as a thin film on plastic (yellow).

Electron diffraction data show that our Co_3O_4 nanoparticles synthesized by PLAL are randomly oriented crystals (see Figure S2).

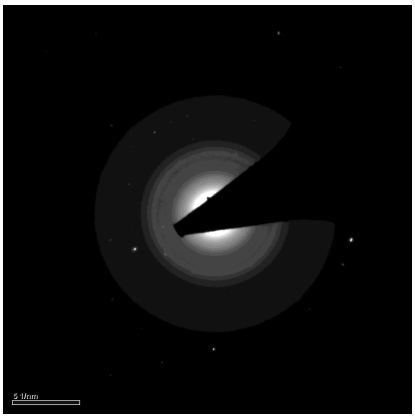

Figure S2: Electron diffraction data of Co_3O_4 nanoparticles synthesized using PLAL at 90 mJ/pulse.

Raman spectroscopy was used to identify the composition of the cobalt oxide nanoparticles. Comparison with two commercially available Co_3O_4 powders of different sizes (10 μm and 50 nm, both Aldrich) showed that our cobalt oxide nanoparticles that were synthesized at four different laser pulse energies are indeed Co_3O_4 (Figure S3). Attempts were made to obtain x-ray diffraction spectra but they were unsuccessful, presumably because such small particles scatter at broad angles, and no defined peaks could be obtained.

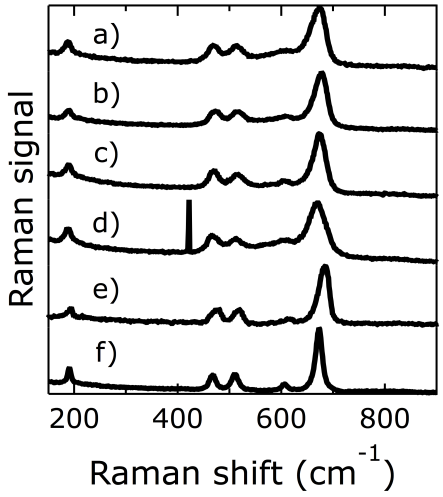

Figure S3: Raman spectra of Co_3O_4 nanoparticles synthesized using PLAL with four different laser pulse energies (a) 30 mJ/pulse, b) 90 mJ/pulse, c) 150 mJ/pulse, d) 210 mJ/pulse; the spike is a cosmic ray event on the detector), and commercially available 50 nm (e) and 10 μm (f) Co_3O_4 powders. For a comparison of Co_3O_4 and CoO Raman spectra, see Gallant, D.; Pézolet, M.; Simard, S. *J. Phys. Chem. B* **2006**, *110*, 6871-6880.

X-ray photoelectron spectra were taken for additional characterization and to compare particle composition before and after anodic cycling in 1.0 M pH 14.0 aqueous KOH electrolyte (Figure S4). After Shirley background subtraction, the Co 2p peaks were fitted and binding energies of 780.3 eV (Co $2p_{3/2}$) and 795.6 eV (Co $2p_{1/2}$) were obtained, which are consistent with published binding energies for Co_3O_4.[5]

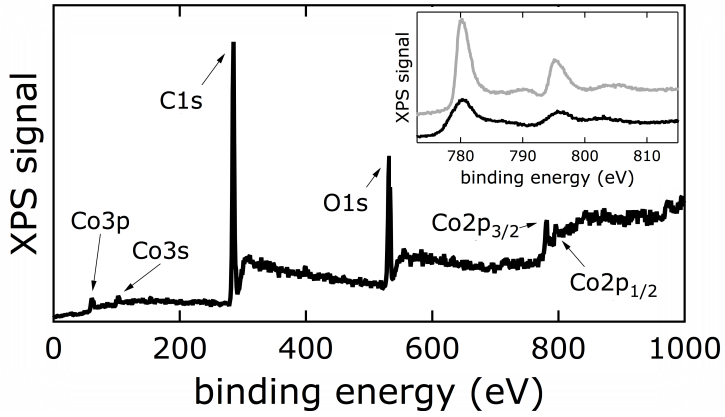

Figure S4: XPS of Co_3O_4 nanoparticles synthesized at 90 mJ/pulse. Inset: Co 2p region, as synthesized (black) and after multiple anodic cycles (gray).

Cobalt concentration in the aqueous Co_3O_4 nanoparticle suspensions was analyzed using inductively-coupled plasma mass spectrometry (ICP-MS) and increases linearly with laser pulse energy (Figure S5).

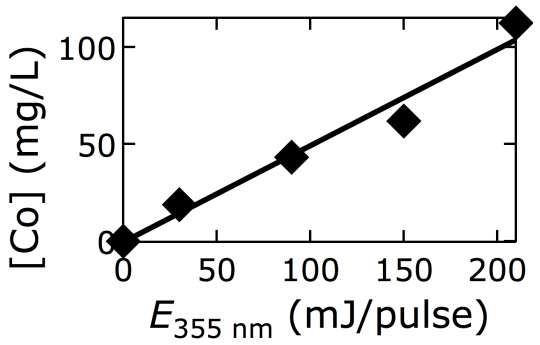

Figure S5: Co concentration vs. laser pulse energy. The solid line is a linear fit.

3. Electrochemical Characterization

We evaluated the electrocatalytic activity of the small Co_3O_4 nanoparticles synthesized by PLAL using cyclic voltammetry in basic water (Figures S6 and S7). Depicted are 10 anodic cycles. Note that the current densities stabilize after the first few cycles.

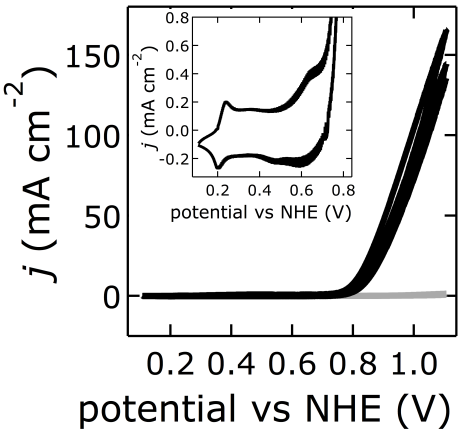

Figure S6: Cyclic voltammograms (10 cycles) of 360 ng Co_3O_4 nanoparticles synthesized at 90 mJ/pulse (black) and bare electrode (gray). The inset depicts a magnification of the second cycle, showing the presence of non-catalytic redox events. Current densities (j) are normalized to geometric electrode areas.

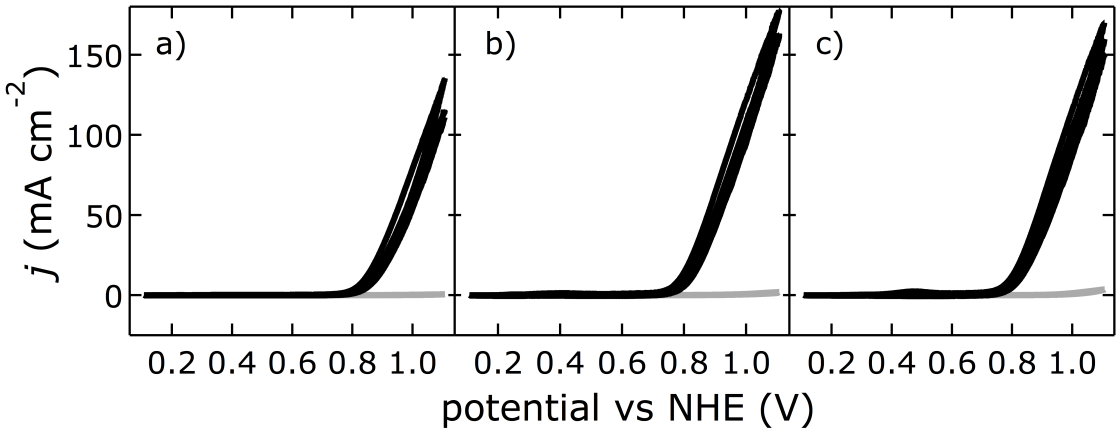

Figure S7: Cyclic voltammograms (10 cycles) of a) 160 ng Co_3O_4 nanoparticles synthesized at 30 mJ/pulse (black), b) 520 ng Co_3O_4 nanoparticles synthesized at 150 mJ/pulse (black), c) 940 ng Co_3O_4 nanoparticles synthesized at 210 mJ/pulse (black); bare electrode cyclic voltammograms are depicted in gray. Current densities (j) are normalized to geometric electrode areas.

In order to assess size changes during anodic cycles, we performed electrochemistry experiments on Co_3O_4 nanoparticles synthesized at 90 mJ/pulse dispersed on TEM grids, washed them well with deionized water, dried them on air, and took TEM images after different numbers of anodic cycles. We observed redox-mediated ripening during the first few cycles and stabilization afterwards (Figure S8).

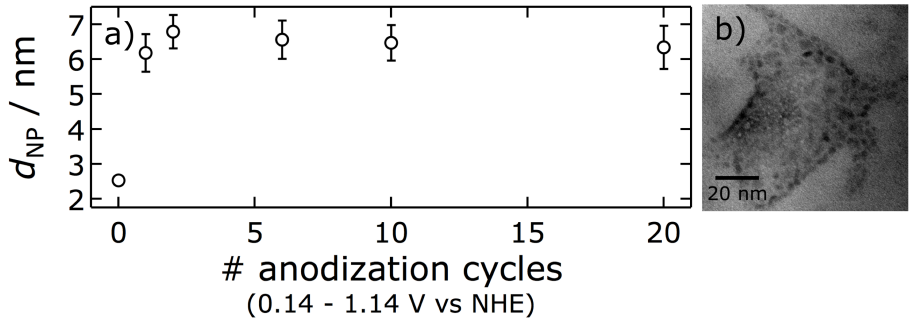

Figure S8: Redox-mediated ripening of Co_3O_4 nanoparticles synthesized at 90 mJ/pulse; a) nanoparticle diameters (d_{NP}) derived from TEM image analysis vs. number of anodic cycles, b) TEM image of Co_3O_4 nanoparticles after 10 anodization cycles.

We also compared catalytic activity of our Co_3O_4 nanoparticles synthesized at 90 mJ/pulse with that of 50-nm bulk Co_3O_4 when normalized to the predicted microscopic Co_3O_4 surface area, while maintaining virtually identical catalyst mass loadings, and find that our small nanoparticles are significantly more active (Figure S9). The surface area A_{calc} of the Co_3O_4 nanoparticles was calculated assuming spherical shape and a mean diameter of the redox-mediated ripened nanoparticles of 6.5 nm (A_{calc} = 0.55 cm^2), while that of the bulk particles was based on spherical shape and 50-nm diameter (A_{calc} = 0.20 cm^2).

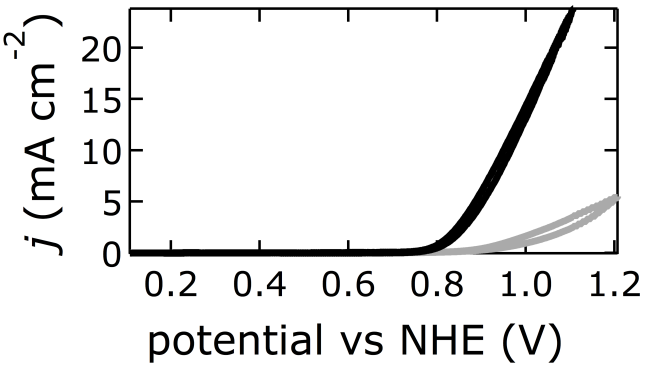

Figure S9: Electrocatalytic activity of 360 ng Co_3O_4 nanoparticles synthesized at 90 mJ/pulse (black) and of 360 ng 50-nm bulk Co_3O_4 (gray). Current densities (j) are normalized to the calculated Co_3O_4 surface areas A_{calc} as described above.

We performed rotating ring-disk electrode (RRDE) electrochemistry experiments, in which oxygen reduction was monitored at the ring electrode during sweeps of the disk electrode voltage through our large catalytic wave (Figure S10). In order to keep everything as comparable as possible, we performed these measurements with virtually the same catalyst mass loading as we used for all other water oxidation catalysis performance assessments. The data collected suggest that oxygen bubbles form even at high rotation speeds. We observed ring currents that are smaller than expected and further decreased over time, presumably due to hydrodynamic effects caused by bubble formation, which was visible by eye. In other words, our catalytic nanoparticles are too active to make use of RRDE for quantification of oxygen evolution under the experimental conditions used.

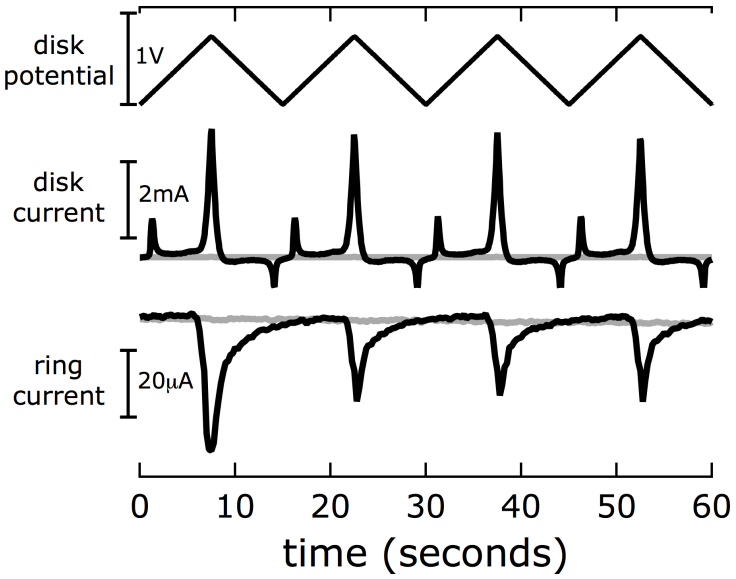

Figure S10: RRDE data of 360 ng Co_3O_4 nanoparticles synthesized at 90 mJ/pulse (black) and bare HOPG electrode (gray).

We measured the amount of oxygen evolved during electrocatalysis using a photoluminescence-quench probe and obtained Faradaic yield of (108±10)%. Again, to keep everything as comparable as possible, we measured the Faradaic yield of oxygen at virtually the same catalyst mass loading as we used for all other water oxidation catalysis performance assessments. The disjointed segments in the measured data seem to have occurred when bubbles were released from the electrode surface; oxygen bubble formation and release inevitably occurred under our experimental conditions due to the high water oxidation activity of the Co_3O_4 nanoparticles. To summarize, we observed production of 7.0 μmol of oxygen, while we predicted 6.5 μmol would be produced based on charge transferred. The predicted and actual oxygen production rates compare well as 212 nmol min^{-1} and 201 nmol min^{-1}, respectively; this indicates essentially quantitative oxygen yield.

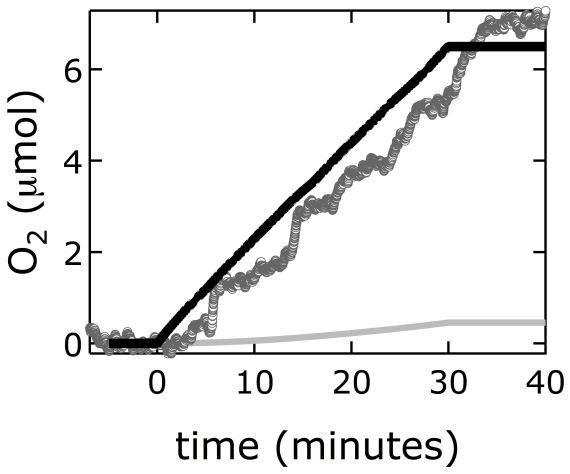

Figure S11: Electrocatalytic production of oxygen. Dark gray: 360 ng Co_3O_4 nanoparticles synthesized at 90 mJ/pulse on an HOPG electrode; black: predicted oxygen evolution based on the total charge transferred; light gray: predicted oxygen evolution without catalyst based on charge transferred.

Long-term stability data were collected with virtually the same catalyst mass loading as for catalytic performance assessment, using a commercial rotating disk electrode electrochemistry instrument as described above. The observed current density was stable beyond 6 hours, indicating that the Co_3O_4 nanoparticles are chemically stable under the experimental conditions used. The jagged nature of the curve arises from oxygen bubble formation and release, which were visible by eye; this does not seem to cause mechanical detachment of the Co_3O_4 nanoparticles from the HOPG electrode surface.

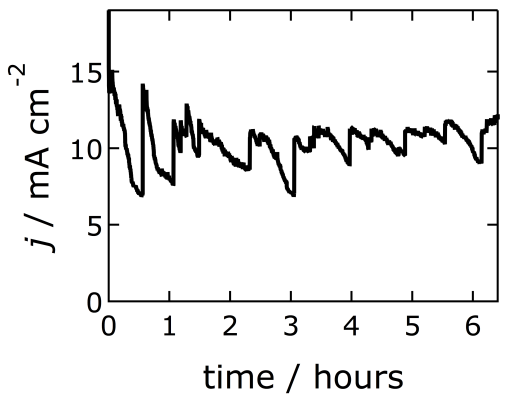

Figure S12: Chronoamperometry data of 360 ng Co_3O_4 nanoparticles synthesized at 90 mJ/pulse on an HOPG electrode.

4. Evidence for Quantum Confinement

We find evidence for quantum confinement in our very small Co_3O_4 nanoparticles synthesized by pulsed laser ablation in liquids. Co_3O_4 nanoparticles with four different mean sizes were synthesized by applying laser pulses with different pulse energies (30, 90, 150, and 210 mJ/pulse). Transmission mode absorption spectra of these Co_3O_4 nanoparticles in solid films compared to those in aqueous suspension are distinctly red-shifted (see Figure S13).

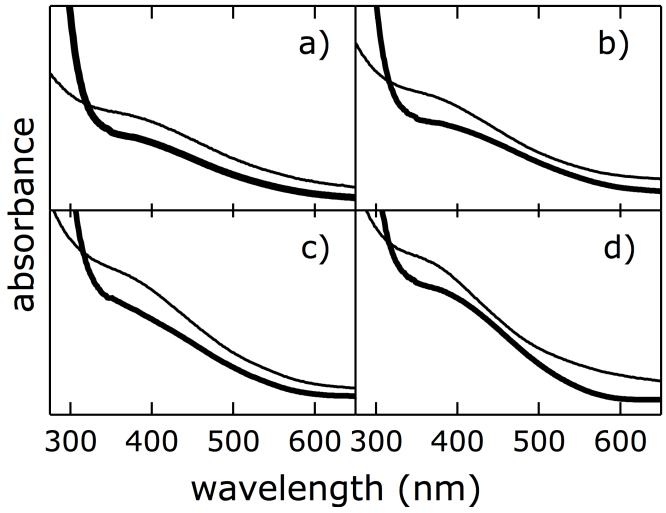

Figure S13: Transmission mode Co_3O_4 nanoparticle absorption spectra in solid films (thick line) and aqueous suspensions (thin line). Irradiation pulse energies: a) 30 mJ/pulse, b) 90 mJ/pulse, c) 150 mJ/pulse, d) 210 mJ/pulse.

Plotting the direct and indirect bandgaps of the Co_3O_4 nanoparticles with four different mean sizes vs. their diameters d reveals a sharp increase of the bandgaps as a function of $1/d^2$ at sizes ≤ ~5 nm (Figure S14). Bandgaps were obtained by Tauc analysis of the absorption spectra of Co_3O_4 nanoparticles in aqueous suspension (Figure S15), and nanoparticle diameters were derived from TEM analysis (Figure S16 and S17).

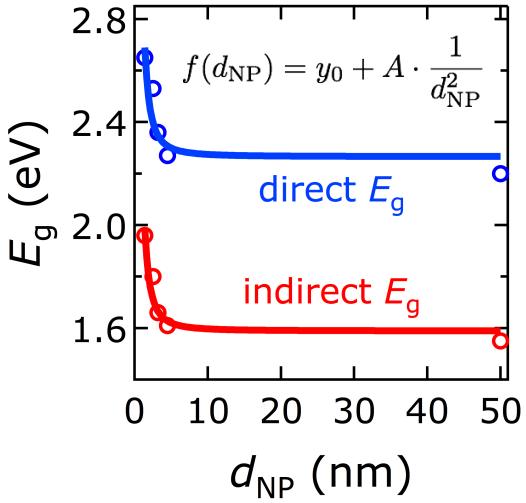

Figure S14: Bandgap (E_g) vs. Co_3O_4 nanoparticle diameter (d_{NP}) plot, indicating quantum confinement at small nanoparticle sizes. Error bars are smaller than the marker sizes. The bulk bandgap energies are from reference Shinde, V. R.; Mahadik, S. B.; Gujar T. P.; Lokhande C. D. *Appl. Surf. Sci.* **2006**, *252*, 7487-7492. The solid lines are fits, using a power law fit function as denoted in the graph, where d_{NP} is the nanoparticle diameter, y_0 is a vertical offset, and A is an amplitude.

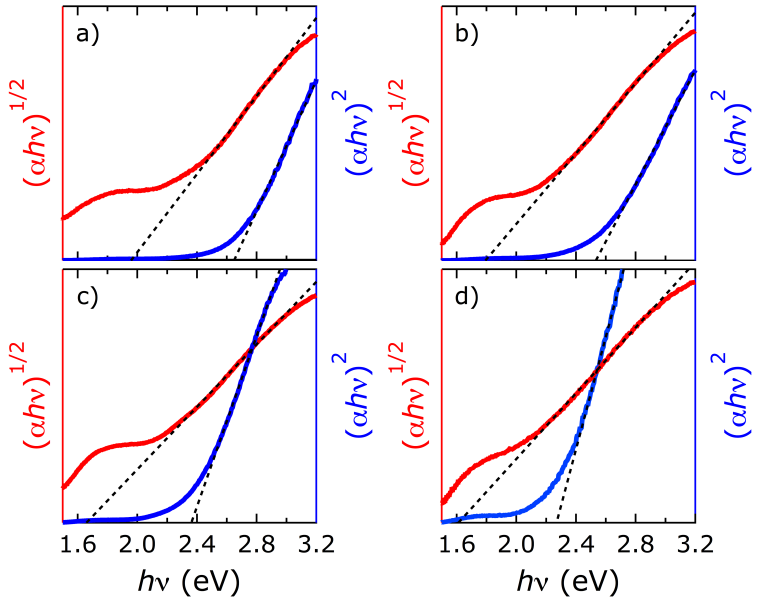

Figure S15: Tauc plots of Co_3O_4 nanoparticles derived from their absorption spectra in aqueous suspension. Red: indirect band gap, blue: direct band gap. Irradiation pulse energies: a) 30 mJ/pulse, b) 90 mJ/pulse, c) 150 mJ/pulse, d) 210 mJ/pulse.

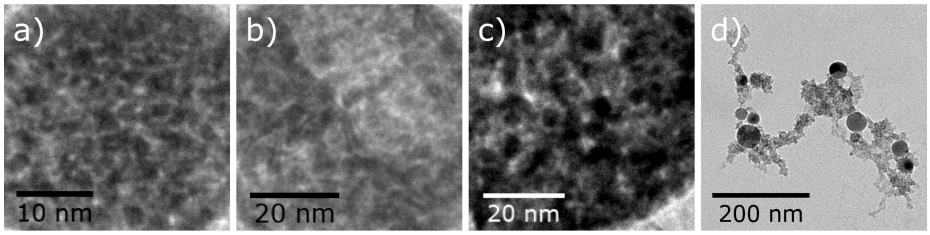

Figure S16: TEM images of Co_3O_4 nanoparticles synthesized at different irradiation pulse energies: a) 30 mJ/pulse, b) 150 mJ/pulse, c) 210 mJ/pulse, d) 90 mJ/pulse (lower magnification). Note that the <5-nm Co_3O_4 nanoparticles are aggregated because PLAL synthesis was performed without addition of stabilizing surfactants, in order to retain full catalytic activity on the nanoparticles' surface. A higher-magnification TEM image of Co_3O_4 nanoparticles synthesized at 90 mJ/pulse is depicted in the main text.

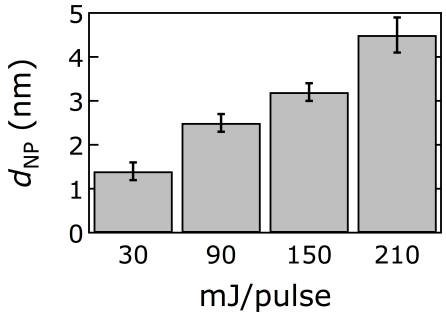

Figure S17: Mean diameters of Co_3O_4 nanoparticles (d_{NP}) synthesized at four different pulse energies.

And lastly, we estimated the critical Co_3O_4 nanoparticle diameter for quantum confinement d_{QC}, which is twice the exciton Bohr radius a_B, using the following equation:

$$a_B = \frac{4\pi\epsilon_0\hbar^2}{m_e e^2} \cdot \frac{\epsilon}{m^*/m_e}$$

In this equation, ε_0 is the permittivity of free space, $\hbar$ is the reduced Planck's constant, m_e is the electron rest mass, e is the elementary charge, ε is the dielectric constant of bulk Co_3O_4, which is 12.9,[6] and m^* denotes the effective mass and is defined as the product of the effective hole and electron masses divided by the sum of the effective hole and electron masses. Since bulk Co_3O_4 is a p-type semiconductor the effective hole mass m_h^* is known ($m_h^* = 0.4\ m_e$)[7] but the effective electron mass is not. Therefore, we estimated it to be half the effective hole mass from analyzing the band structure of bulk Co_3O_4, which shows stronger delocalization in the conduction band than in the valence band.[8] As a result we obtained a critical quantum confinement diameter of 4.9 nm.

References:

[1] Kanan, M. W.; Nocera, D. G. *Science* **2008**, *321*, 1072-1075.
[2] Rasband, W. S. ImageJ; U. S. National Institutes of Health: Bethesda, MD. Available online at http://imagej.nih.gov/ij/.
[3] Solla-Gullon, J.; Vidal-Iglesias, F. J.; Lopez-Cudero, A.; Garnier, E.; Feliu, J. M.; Aldaz, A. *Phys. Chem. Chem. Phys.* **2008**, *10*, 3689-3698.
[4] James R. McKone, *personal communication.*
[5] Petitto, S. C.; Langell, M. A. *J. Vac. Sci. Technol., A* **2004**, *22*, 1690-1696.
[6] Rao, K. V.; Smakula, A., *J. Appl. Phys.* **1965**, *36*, 2031-2038.
[7] Cheng, C.-S.; Serizawa, M.; Sakata, H.; Hirayama, T. *Mater. Chem. Phys.* **1998**, *53*, 225-230.
[8] Chen, J.; Wu, X.; Selloni, A. *Phys. Rev. B: Condens. Matter Mater. Phys.* **2011**, *83*, 245204/245201-245204/245207.